Malaysian Journal of Mathematical Sciences 19(2): 595–611 (2025)
https://doi.org/10.47836/mjms.19.2.12

Malaysian Journal of Mathematical Sciences

Journal homepage: https://mjms.upm.edu.my

Rotating Thermosolutal Convection for the Darcy-Brinkman Model with Variable Gravity and Chemical Reaction Influences

Noon, N. J.* [1]

[1] *Department of Mathematics, the Directorate of Education in Basra Governorate, Iraq*

E-mail: najatj.noon@gmail.com
**Corresponding author*

Received: 4 April 2024
Accepted: 26 December 2024

Abstract

The effect of varying gravity and chemical reaction on rotating thermosolutal convection in a Darcy-Brinkman porous substance is tested. The linear instability theory based on fixed border conditions when the layer is heated and salted from below has been employed. Three forms of varying gravitational are discussed: linear function, parabolic function, and exponential function. The related system has been solved by applying the D^2 Chebyshev-Tau technique. Against the influence of varying gravity, rotation, Brinkman coefficient, chemical reaction, and salt Rayleigh number, the critical Rayleigh number has been graphically displayed. In addition, the results indicate that the investigated impacts have a significant impact on locating the convection instability threshold.

Keywords: rotating thermosolutal convection; Darcy-Brinkman model; variable gravity effect and chemical reaction effect.

1 Introduction

The phenomenon of thermosolutal convection is crucial to the dynamics of fluids that arise when two distinct gradients of density (like salinity and temperature) with different diffusion rates interact [5]. Thermosolutal convection in a porous substance has grown more important in recent years as a result of its numerous applications in various real-life situations, such as waste disposal, contaminated groundwater, and so on [8]. The spread of pollutants and contaminants in soils, shallow water layers, and shallow atmospheres is an area of intense interest in research that has applications to several geophysical environmental issues of contemporary life [4]. Moreover, in both Newtonian and non-Newtonian fluids, thermosolutal convection is an important concept that is investigated both practically and theoretically [6]. Furthermore, several authors have focused their attention on convection with varying gravity, rotation, and chemical reaction effects; for example, the sufficient and necessary conditions of unconditional stability on rotating thermosolutal convection in a Darcy-Brinkman porous were studied in [7]. The outcomes were generalized to those obtained by Straughan [14] for the Darcy system in thermal convection. The findings were derived for free border conditions using the Lyapunov direct technique and demonstrated the stabilizing influence of rotation on the onset of convection.

For the Darcy system based on free border conditions, [15] used the Galerkin-weighted residual scheme to investigate the impact of varied gravity and rotation on thermal convection. The outcomes revealed that the gravity variation and rotation impacts slowed the onset of convection, and as the gravity variation and rotation values grew, the convection cells' measurement was reduced. In [10], the influence of altered gravitation and chemical reaction on rotating thermosolutal convection for the Darcy equation in a porous substance with free boundary conditions was discussed as the surface layer was salted from either the top or bottom, and heated from the bottom. The linear function, the parabolic function, and the exponential function of altered gravitation were examined. They demonstrated that combining the effects of variable gravitation and rotation as well as the chemical-reaction influence had a considerable effect on defining the convection instability threshold. The influence of altered gravitation together with the chemical-reaction and internally heated source impacts on thermosolutal convection in a porous material for the Darcy-Brinkman problem with slip border conditions was tested in [9], as the surface layer had been salted from either the top or bottom and heated from the bottom. Three functions of the interior heat source and varying gravity have been examined. The outcomes demonstrated that combining the influence of altered gravitation and chemical-reaction with the internally heated source influence and slip border conditions had a noteworthy influence on measuring the convection instability threshold.

The Chebyshev-collocation procedure was used in [11] to study the magnetic impact, heat interior source impact, and chemical reaction impact on thermosolutal convection when the underside layer has particular heat and salt fluxes. Given the findings, controlling the limits for thermosolutal convection destabilization and stabilization is substantially affected using magnetic, heat interior sources, and chemical reactions. In [13, 1], the Galerkin manner was used to study the gravitational impacts in the absence and presence of rotation impact, respectively, on the thermal-convection porous surface of Jeffrey nanofluid for the Darcy-Brinkman system in free borders. It was revealed that the gravitational coefficient with a negative exponent fluctuation stabilizes both stationary and oscillatory convections more effectively.

The linear instability threshold for rotating thermosolutal convection involving varying gravitation and chemical-reaction influences for the Darcy-Brinkman problem in a porous substance has been discussed in this work. The goal of this article is to investigate the system's instability analysis with fixed boundary conditions, along with the impacts of rotation, varying gravity, and chemical-reaction. Three functions of variable gravity have been discussed: the linear function, the parabolic function, and the exponential function. The D^2 Chebyshev-Tau technique is applied to analyze linear instability theory. To this end, Section 2 provides the basic equations and steady-state solutions. Section 3 analyzes linear instability theory. Section 4 discusses the D^2 Chebyshev-Tau approach to solving an eigenvalue system. Section 5 illustrates graphically the critical Rayleigh number against the impacts of varying downward gravity, chemical reaction, Brinkman coefficient, and salt Rayleigh number. Section 6 provides the conclusion.

2 Governing Equations

Assume a porous fluid-saturated layer is rotating across a vertical axis z and is bordered by the horizontal axes, $\{(x, y) \in \mathbb{R}^2 \times z \in (0, d)\}$. In thermosolutal convection, the Darcy-Brinkman model is used, which allows gravity g to be fixed by the axis z, as illustrated in Figure 1.

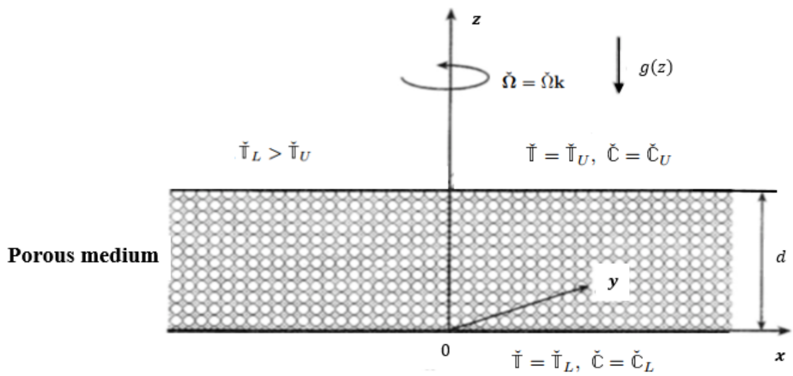

Figure 1: The physical presentation of rotational thermosolutal convection.

$$
\begin{aligned}
0 &= -\frac{\mu}{K}\breve{\mathbb{v}}_i - \breve{\mathbb{p}}_{,i} + \Big[-\rho_0 g(z) + \rho_0 \alpha_{\breve{\mathbb{T}}} g(z)(\breve{\mathbb{T}} - \breve{\mathbb{T}}_0) - \rho_0 \alpha_{\breve{\mathbb{C}}} g(z)(\breve{\mathbb{C}} - \breve{\mathbb{C}}_0) \Big] k_i \\
&\quad + \lambda \Delta\, \breve{\mathbb{v}}_i - 2\frac{\rho_0}{\epsilon}(\breve{\mathbf{\Omega}} \times \breve{\mathbb{v}}_i), \\
0 &= \breve{\mathbb{v}}_{i,i}, \\
0 &= \frac{1}{\mathbb{M}}\breve{\mathbb{T}}_{,t} - k_{\breve{\mathbb{T}}} \Delta \breve{\mathbb{T}} + \breve{\mathbb{v}}_i \breve{\mathbb{T}}_{,i}, \\
0 &= \hat{\varphi}\breve{\mathbb{C}}_{,t} - \hat{\varphi} k_{\breve{\mathbb{C}}} \Delta \breve{\mathbb{C}} + \breve{\mathbb{v}}_i \breve{\mathbb{C}}_{,i} - \hat{k}\breve{\mathbb{C}}_{eq}(\breve{\mathbb{T}}) + \hat{k}\,\breve{\mathbb{C}},
\end{aligned} \tag{1}
$$

where $\breve{\mathbb{v}}_i$ is the velocity, $\breve{\mathbb{p}}$ is the pressure, $\breve{\mathbb{T}}$ is the temperature, $\breve{\mathbb{C}}_{eq}$ is the solute's equilibrium concentration at a specific $\breve{\mathbb{T}}$, and $\breve{\mathbb{C}}$ is the concentration's salt. μ and λ are viscosities, g is the gravity, ρ_0 is the fluid's density at the reference temperature $\breve{\mathbb{T}}_0$. $\alpha_{\breve{\mathbb{T}}}$ is the thermal expansion coefficient, $\alpha_{\breve{\mathbb{C}}}$ is the coefficient of the solute's expansion, ϵ is the porosity, $k_{\breve{\mathbb{T}}}$ represents the heat's effective diffusivity across the saturated material, $k_{\breve{\mathbb{C}}}$ is the solute's molecular diffusivity across the fluid, $\hat{k}$ is the reaction coefficient, $\mathfrak{M}$ denotes the proportion between the fluid's and the medium's heat capacities, and $\hat{\varphi}$ is the porosity of the matrix, $\breve{\mathbf{\Omega}} = \breve{\Omega}\mathbf{k}$ indicates the rotation's angular velocity field, where $\mathbf{k} = (0, 0, 1)$.

In [12], the $\breve{\mathbb{C}}_{eq}$ is supposed as a linear function of $\breve{\mathbb{T}}$ such that $\breve{\mathbb{C}}_{eq}(\breve{\mathbb{T}}) = \breve{\mathbb{f}}_1(\breve{\mathbb{T}} - \breve{\mathbb{T}}_0) + \breve{\mathbb{f}}_0$, where

$\check{\mathbb{T}}_0, \check{\mathbb{f}}_0$, and $\check{\mathbb{f}}_1$ are constants. The conditions for borders are:

$$\begin{aligned} &0 = \check{\mathbb{v}}_i, && \text{at} \quad z = d, 0, \\ &\check{\mathbb{T}} = \check{\mathbb{T}}_L, && \text{at} \quad z = 0, \qquad \check{\mathbb{T}} = \check{\mathbb{T}}_U, \quad \text{at} \quad z = d, \\ &\check{\mathbb{C}} = \check{\mathbb{C}}_L, && \text{at} \quad z = 0, \qquad \check{\mathbb{C}} = \check{\mathbb{C}}_U \quad \text{at} \quad z = d, \end{aligned} \tag{2}$$

where the system is salted and heated bottom (i.e. $\check{\mathbb{C}}_L > \check{\mathbb{C}}_U$ and $\check{\mathbb{T}}_L > \check{\mathbb{T}}_U$) and $\check{\mathbb{C}}_U, \check{\mathbb{C}}_L, \check{\mathbb{T}}_U$ and $\check{\mathbb{T}}_L$ are constants. For a steady state, seek,

$$\bar{\bar{\mathbb{v}}}_i = 0, \qquad \bar{\bar{\check{\mathbb{T}}}} = \bar{\bar{\check{\mathbb{T}}}}(z), \qquad \bar{\bar{\check{\mathbb{C}}}} = \bar{\bar{\check{\mathbb{C}}}}(z).$$

From [12], by assuming $\check{\mathbb{C}}_{eq}(\bar{\bar{\check{\mathbb{T}}}}) = \bar{\bar{\check{\mathbb{C}}}}(z)$, the steady solution is found to (1) which satisfies (2) as,

$$\bar{\bar{\mathbb{v}}}_i = 0, \qquad \bar{\bar{\check{\mathbb{T}}}} = -\beta_{\check{\mathbb{T}}} z + \check{\mathbb{T}}_L, \qquad \bar{\bar{\check{\mathbb{C}}}} = -\beta_{\check{\mathbb{C}}} z + \check{\mathbb{C}}_L, \tag{3}$$

where $\beta_{\check{\mathbb{T}}} = \dfrac{(\check{\mathbb{T}}_L - \check{\mathbb{T}}_U)}{d}$ and $\beta_{\check{\mathbb{C}}} = \dfrac{(\check{\mathbb{C}}_L - \check{\mathbb{C}}_U)}{d}$. For analyzing the solution's stability of (3), find the perturbations $(\check{\mathbb{u}}_i, \check{\pi}, \check{\theta}, \check{\phi})$ so that,

$$\check{\mathbb{v}}_i = \check{\mathbb{u}}_i + \bar{\bar{\mathbb{v}}}_i, \qquad \check{\mathbb{p}} = \check{\pi} + \bar{\bar{\mathbb{p}}}, \qquad \check{\mathbb{T}} = \check{\theta} + \bar{\bar{\check{\mathbb{T}}}}, \qquad \check{\mathbb{C}} = \check{\phi} + \bar{\bar{\check{\mathbb{C}}}}.$$

The governing equations can be derived by incorporating these perturbations into (1),

$$\begin{aligned} &0 = -\frac{\mu}{K}\check{\mathbb{u}}_i - \check{\pi}_{,i} + g(z)\alpha_{\check{\mathbb{T}}}\check{\theta}\rho_0 k_i - g(z)\alpha_{\check{\mathbb{C}}}\check{\phi}\rho_0 k_i + \lambda\Delta\,\check{\mathbb{u}}_i - 2\frac{\rho_0}{\epsilon}(\boldsymbol{\Omega} \times \check{\mathbb{u}}_i), \\ &0 = \check{\mathbb{u}}_{i,i}, \\ &0 = \frac{1}{\mathbb{M}}\check{\theta}_{,t} - \beta_{\check{\mathbb{T}}}\check{\mathbb{w}} + \check{\mathbb{u}}_i\check{\theta}_{,i} - k_{\check{\mathbb{T}}}\Delta\check{\theta}, \\ &0 = \hat{\varphi}\check{\phi}_{,t} - \beta_{\check{\mathbb{C}}}\check{\mathbb{w}} + \check{\mathbb{u}}_i\check{\phi}_{,i} - \hat{\varphi}k_{\check{\mathbb{C}}}\Delta\check{\phi} - \hat{k}\check{\mathbb{f}}_1\check{\theta} + \hat{k}\check{\phi}, \end{aligned} \tag{4}$$

where $\check{\mathbb{u}}_i = \{\check{\mathbb{u}}, \check{\mathbb{v}}, \check{\mathbb{w}}\}$. Equation (4) is non-dimensionalized with the transformations, $x = dx^*$, $t = \dfrac{d^2}{\mathbb{M}k_{\check{\mathbb{T}}}}$, $\check{\mathbb{u}} = \dfrac{k_{\check{\mathbb{T}}}}{d}\check{\mathbb{u}}^*$, $\check{\pi} = \dfrac{k_{\check{\mathbb{T}}}\mu}{K}\check{\pi}^*$, $\check{\check{\mathbb{T}}} = \sqrt{\dfrac{\mu\beta_{\check{\mathbb{T}}}k_{\check{\mathbb{T}}}}{\alpha_{\check{\mathbb{T}}}\rho_0 g K}}$, $\check{\theta} = \check{\check{\mathbb{T}}}\check{\theta}^*$, $\check{\check{\mathbb{C}}} = \sqrt{\dfrac{\mu\beta_{\check{\mathbb{C}}}k_{\check{\mathbb{C}}}Le}{\alpha_{\check{\mathbb{C}}}\rho_0 g K\hat{\varphi}}}$, $\check{\phi} = \check{\check{\mathbb{C}}}\check{\phi}^*$, $R = \sqrt{\dfrac{\beta_{\check{\mathbb{T}}}d^2K\alpha_{\check{\mathbb{T}}}\rho_0 g}{k_{\check{\mathbb{T}}}\mu}}$ is the temperature number, $R_s = \sqrt{\dfrac{\beta_{\check{\mathbb{C}}}d^2K\alpha_{\check{\mathbb{C}}}\rho_0 g Le}{\hat{\varphi}k_{\check{\mathbb{T}}}\mu}}$ is the salt Rayleigh number, and the Lewis number is $Le = \dfrac{k_{\check{\mathbb{T}}}}{k_{\check{\mathbb{C}}}}$.

By removing stars, the system of non-dimensional perturbations is,

$$\begin{aligned} &0 = -\check{\mathbb{u}}_i - \check{\pi}_{,i} + RH_1(z)k_i\check{\theta} - R_s H_1(z)k_i\check{\phi} + \tilde{\gamma}\Delta\,\check{\mathbb{u}}_i - \check{T}_a(K \times \check{\mathbb{u}}_i), \\ &0 = \check{\mathbb{u}}_{i,i}, \\ &0 = \check{\theta}_{,t} - R\check{\mathbb{w}} + \check{\mathbb{u}}_i\check{\theta}_{,i} - \Delta\check{\theta}, \\ &0 = \epsilon\check{\phi}_{,t} - R_s\check{\mathbb{w}} + \frac{Le}{\hat{\varphi}}\check{\mathbb{u}}_i\check{\phi}_{,i} - \Delta\check{\phi} + \eta\check{\phi} - h\check{\theta}, \end{aligned} \tag{5}$$

where $H_1(z) = 1 + \alpha h_1(z)$, where $g(z) = g(1 + \alpha h_1(z))$, g constant, $h_1(z)$, is the function that estimates the inconsistencies of the gravitational field, and α is the varying gravitation factor. $\tilde{\gamma} = \dfrac{\lambda K}{\mu d^2}$

is the Brinkman coefficient, $\epsilon = \mathbb{M}Le$, the Taylor number is $\breve{T}_a = \dfrac{2\rho_0 K\breve{\Omega}}{\epsilon\mu}$, and the reaction terms are $h = \dfrac{\hat{k}\breve{\mathbb{f}}_1\breve{\breve{\mathbb{T}}}}{\hat{\varphi}k_{\breve{\mathbb{C}}}\breve{\breve{\mathbb{C}}}}$ and $\eta = \dfrac{\hat{k}d^2}{\hat{\varphi}k_{\breve{\mathbb{C}}}}$. Equation (5) can be held in $\big\{\{(x,y)\in\mathbb{R}^2\}\times\{z\in(0,1)\}\times\{t>0\}\big\}$, where the borders have been represented as,

$$\breve{\mathbb{w}} = \breve{\mathbb{w}}_z = 0, \qquad \breve{\theta} = 0, \qquad \breve{\phi} = 0, \qquad \text{at} \qquad z = 0, 1,$$

in the fixed surfaces case and,

$$\breve{\mathbb{w}} = \breve{\mathbb{w}}_{zz} = 0, \qquad \breve{\theta} = 0, \qquad \breve{\phi} = 0, \qquad \text{at} \qquad z = 0, 1,$$

in the free surfaces case.

3 The Theory of Linear Instability

At this stage, the definition of a vorticity domain $\breve{\omega}(x)$ must be introduced, which provides a measurement of the fluid's rotation as follows,

$$\nabla \times \breve{\mathbb{u}}_i = \breve{\omega}_i(x).$$

Using the 3rd component of curl and curl curl for $(5)_1$ gives,

$$\begin{aligned}
0 &= -\breve{\omega}_3 + \tilde{\gamma}\Delta\,\breve{\omega}_3 + \breve{T}_a\breve{\mathbb{w}}_z,\\
0 &= \Delta\breve{\mathbb{w}} - \tilde{\gamma}\Delta^2\,\breve{\mathbb{w}} + \breve{T}_a\breve{\omega}_{3,z} - RH_1(z)\Delta^*\breve{\theta} + R_sH_1(z)\Delta^*\breve{\phi},\\
0 &= \breve{\theta}_{,t} - R\breve{\mathbb{w}} + \breve{\mathbb{u}}_i\breve{\theta}_{,i} - \Delta\breve{\theta},\\
0 &= \epsilon\breve{\phi}_{,t} - R_s\breve{\mathbb{w}} + \frac{Le}{\hat{\varphi}}\breve{\mathbb{u}}_i\breve{\phi}_{,i} - \Delta\breve{\phi} + \eta\breve{\phi} - h\breve{\theta},
\end{aligned} \tag{6}$$

where $\Delta^* = \dfrac{\partial^2}{\partial x^2} + \dfrac{\partial^2}{\partial y^2}$. By dropping the non-linear terms of $(6)_2$ and $(6)_3$, and therefore after seeking the solutions as the following,

$$\begin{aligned}
\breve{\mathbb{w}}(x,t) &= \exp(\breve{\sigma}t)\breve{\mathbb{w}}(x), &\qquad \breve{\omega}_3(x,t) &= \exp(\breve{\sigma}t)\,\breve{\omega}_3(x),\\
\breve{\phi}(x,t) &= \exp(\breve{\sigma}t)\,\breve{\phi}(x), &\qquad \breve{\theta}(x,t) &= \exp(\breve{\sigma}t)\,\breve{\theta}(x),
\end{aligned}$$

where $\breve{\sigma}$ represents the growth rate that depends on time. Consequently, the linearization system resulting from (6) is,

$$\begin{aligned}
0 &= -\breve{\omega}_3 + \tilde{\gamma}\Delta\,\breve{\omega}_3 + \breve{T}_a\breve{\mathbb{w}}_z,\\
0 &= \Delta\breve{\mathbb{w}} - \tilde{\gamma}\Delta^2\,\breve{\mathbb{w}} + \breve{T}_a\breve{\omega}_{3,z} - RH_1(z)\Delta^*\breve{\theta} + R_sH_1(z)\Delta^*\breve{\phi},\\
0 &= \breve{\sigma}\breve{\theta} - R\breve{\mathbb{w}} - \Delta\breve{\theta},\\
0 &= \epsilon\breve{\sigma}\breve{\phi} - R_s\breve{\mathbb{w}} - \Delta\breve{\phi} - h\breve{\theta}.
\end{aligned} \tag{7}$$

Equation (7) can be analyzed by employing standard-methods, refer to [2]. The expressions for $\breve{\mathbb{w}}$, $\breve{\omega}_3$, $\breve{\theta}$ and $\breve{\phi}$ are,

$$\breve{\mathbb{w}} = \breve{\mathbb{f}}(x,y)\breve{\mathbb{W}}(z), \qquad \breve{\omega}_3 = \breve{\mathbb{f}}(x,y)\varpi(z), \qquad \breve{\theta} = \breve{\mathbb{f}}(x,y)\breve{\Theta}(z), \qquad \breve{\phi} = \breve{\mathbb{f}}(x,y)\breve{\Phi}(z),$$

where $\check{\mathbb{f}}$ is a horizontal plan form that fulfills $\Delta^*\check{\mathbb{f}} = -\check{\mathfrak{a}}^2\check{\mathbb{f}}$, $\check{\mathfrak{D}} = \dfrac{d}{dz}$, $\check{\mathfrak{a}}$ is a wave-number and $\Delta = \check{\mathfrak{D}}^2 - \check{\mathfrak{a}}^2$, (7) can be represented as,

$$\begin{aligned}
&0 = -\varpi + \tilde{\gamma}(\check{\mathfrak{D}}^2 - \check{\mathfrak{a}}^2)\,\varpi + \check{T}_a\,\check{\mathfrak{D}}\check{\mathbb{W}},\\
&0 = -\tilde{\gamma}(\check{\mathfrak{D}}^2 - \check{\mathfrak{a}}^2)^2\,\check{\mathbb{W}} + (\check{\mathfrak{D}}^2 - \check{\mathfrak{a}}^2)\check{\mathbb{W}} + \check{T}_a\,\check{\mathfrak{D}}\varpi + RH_1(z)\check{\mathfrak{a}}^2\check{\Theta} - R_sH_1(z)\check{\mathfrak{a}}^2\check{\Phi},\\
&0 = \check{\sigma}\check{\Theta} - (\check{\mathfrak{D}}^2 - \check{\mathfrak{a}}^2)\check{\Theta} - R\check{\mathbb{W}},\\
&0 = \epsilon\check{\sigma}\check{\Phi} - (\check{\mathfrak{D}}^2 - \check{\mathfrak{a}}^2)\check{\Phi} + \eta\check{\Phi} - R_s\check{\mathbb{W}} - h\check{\Theta}.
\end{aligned} \tag{8}$$

With the following border conditions,

$$\check{\mathbb{W}} = \check{\mathfrak{D}}\check{\mathbb{W}} = \varpi = 0, \qquad \check{\Theta} = 0, \qquad \check{\Phi} = 0, \quad \text{at} \quad z = 0, 1, \tag{9}$$

in the fixed surfaces case and,

$$\check{\mathbb{W}} = \check{\mathfrak{D}}^2\check{\mathbb{W}} = \check{\mathfrak{D}}\varpi = 0, \qquad \check{\Theta} = 0, \qquad \check{\Phi} = 0, \quad \text{at} \quad z = 0, 1, \tag{10}$$

in the free surfaces case. Here, the critical Rayleigh number is determined by,

$$Ra = \min_{\check{\mathfrak{a}}^2} R^2(\check{\mathfrak{a}}^2),$$

where $\forall\ R^2 > Ra$ the instability's system is fulfilled.

4 Numerical Method

For solving the linear instability (8) according to the boundary condition (9), the D^2-Chebyshev-Tau method [3] has been applied in this section. To begin, reset the interval from $0 < z < 1$ to $-1 < z < 1$ by putting $2z - 1 = z^\star$. In addition, $(8)_2$ can be written as a 2nd-order equation by setting,

$$\check{\chi} = (4\check{\mathfrak{D}}^2 - \check{\mathfrak{a}}^2)\check{\mathbb{W}}.$$

Then, by removing the star, (8) can be rewritten as the following,

$$\begin{aligned}
&0 = (4\check{\mathfrak{D}}^2 - \check{\mathfrak{a}}^2)\check{\mathbb{W}} - \check{\chi},\\
&0 = -\varpi + \tilde{\gamma}(4D^2 - a^2)\,\varpi + 2\check{T}_a\,\check{\mathfrak{D}}\check{\mathbb{W}},\\
&0 = \check{\chi} - \tilde{\gamma}(4\check{\mathfrak{D}}^2 - \check{\mathfrak{a}}^2)\check{\chi} + 2\check{T}_a\,\check{\mathfrak{D}}\varpi + RH_2\check{\mathfrak{a}}^2\check{\Theta} - R_sH_2\check{\mathfrak{a}}^2\check{\Phi},\\
&0 = \check{\sigma}\check{\Theta} - (4\check{\mathfrak{D}}^2 - \check{\mathfrak{a}}^2)\check{\Theta} - R\check{\mathbb{W}},\\
&0 = \epsilon\check{\sigma}\check{\Phi} - (4\check{\mathfrak{D}}^2 - \check{\mathfrak{a}}^2)\check{\Phi} - R_s\check{\mathbb{W}} + \eta\check{\Phi} - h\check{\Theta},
\end{aligned} \tag{11}$$

where $H_2 = H_1\left(\frac{z+1}{2}\right)$, $z \in (-1,1)$. Chebyshev polynomials have been employed to expand the functions $\check{\mathbb{W}}, \check{\chi}, \varpi, \check{\Theta}$, and $\check{\Phi}$ as follows,

$$\sum_{n=1}^{M} \hat{\mathbb{T}}_n(z)\, \check{\mathbb{W}}_n = \check{\mathbb{W}}(z),$$
$$\sum_{n=1}^{M} \hat{\mathbb{T}}_n(z)\, \check{\chi}_n = \check{\chi}(z),$$
$$\sum_{n=1}^{M} \hat{\mathbb{T}}_n(z)\, \varpi_n = \varpi(z),$$
$$\sum_{n=1}^{M} \hat{\mathbb{T}}_n(z)\check{\Theta}_n = \check{\Theta}(z),$$
$$\sum_{n=1}^{M} \hat{\mathbb{T}}_n(z)\, \check{\Phi}_n = \Phi(z).$$

Therefore, (11) can be rewritten as follows,

$$\mathbb{A}\check{\mathbb{X}} = \check{\sigma}\mathbb{B}\check{\mathbb{X}}, \tag{12}$$

where $\check{\mathbb{X}} = \left\{\check{\mathbb{W}}_1, \check{\mathbb{W}}_2, \ldots, \check{\mathbb{W}}_M, \check{\chi}_1, \check{\chi}_2, \ldots, \check{\chi}_M, \varpi_1, \varpi_2, \ldots, \varpi_M, \check{\Theta}_1, \check{\Theta}_2, \ldots, \check{\Theta}_M, \check{\Phi}_1, \check{\Phi}_2, \ldots, \check{\Phi}_M\right\}$ and

$$A = \begin{pmatrix} 4\check{\mathfrak{D}}^2 - \check{\mathfrak{a}}^2 I & -I & \mathbf{0} & \mathbf{0} & \mathbf{0} \\ 2\check{T}_a\, D & \mathbf{0} & \tilde{\gamma}(4\check{\mathfrak{D}}^2 - \check{\mathfrak{a}}^2 I) - I & \mathbf{0} & \mathbf{0} \\ \mathbf{0} & -\tilde{\gamma}(4\check{\mathfrak{D}}^2 - \check{\mathfrak{a}}^2 I) + I & 2\check{T}_a\, \check{\mathfrak{D}} & H_2\check{\mathfrak{a}}^2 RI & -H_2\check{\mathfrak{a}}^2 R_s I \\ RI & \mathbf{0} & \mathbf{0} & 4\check{\mathfrak{D}}^2 - \check{\mathfrak{a}}^2 I & \mathbf{0} \\ R_s I & \mathbf{0} & \mathbf{0} & hI & 4\check{\mathfrak{D}}^2 - \check{\mathfrak{a}}^2 I - \eta I \end{pmatrix},$$

$$B = \begin{pmatrix} \mathbf{0} & \mathbf{0} & \mathbf{0} & \mathbf{0} & \mathbf{0} \\ \mathbf{0} & \mathbf{0} & \mathbf{0} & \mathbf{0} & \mathbf{0} \\ \mathbf{0} & \mathbf{0} & \mathbf{0} & \mathbf{0} & \mathbf{0} \\ \mathbf{0} & \mathbf{0} & \mathbf{0} & I & \mathbf{0} \\ \mathbf{0} & \mathbf{0} & \mathbf{0} & \mathbf{0} & \epsilon I \end{pmatrix}.$$

By applying $\hat{\mathbb{T}}'_n(\pm 1) = (\pm 1)^{n-1} n^2$ and $\hat{\mathbb{T}}_n(\pm 1) = (\pm 1)^n$ to fixed border conditions (9), then,

$$
\begin{aligned}
&0 = \sum_{n=1}^{M} \hat{\mathbb{T}}_n(1)\check{\mathbb{W}}_n(1) = \check{\mathbb{W}}(1), && 0 = \sum_{n=1}^{M} \hat{\mathbb{T}}_n(-1)\check{\mathbb{W}}_n(-1) = \check{\mathbb{W}}_n(-1),\\
&0 = \sum_{n=1}^{M} \hat{\mathbb{T}}'_n(1)\check{\mathbb{W}}_n(1) = \check{\mathfrak{D}}\check{\mathbb{W}}(1), && 0 = \sum_{n=1}^{M} \hat{\mathbb{T}}'_n(-1)\check{\mathbb{W}}_n(-1) = \check{\mathfrak{D}}\check{\mathbb{W}}(-1),\\
&0 = \sum_{n=1}^{M} \hat{\mathbb{T}}_n(1)\varpi_n(1) = \varpi(1), && 0 = \sum_{n=1}^{M} \hat{\mathbb{T}}_n(-1)\varpi_n(-1) = \varpi(-1),\\
&0 = \sum_{n=1}^{M} \hat{\mathbb{T}}_n(1)\check{\Theta}_n(1) = \check{\Theta}(1), && 0 = \sum_{n=1}^{M} \hat{\mathbb{T}}_n(-1)\check{\Theta}_n(-1) = \check{\Theta}(-1),\\
&0 = \sum_{n=1}^{M} \hat{\mathbb{T}}_n(1)\check{\Phi}_n(1) = \check{\Phi}(1), && 0 = \sum_{n=1}^{M} \hat{\mathbb{T}}_n(-1)\check{\Phi}_n(-1) = \check{\Phi}(-1).
\end{aligned}
\tag{13}
$$

And for free border conditions (10), then,

$$
\begin{aligned}
&0 = \sum_{n=1}^{M} \hat{\mathbb{T}}_n(1)\check{\mathbb{W}}_n(1) = \check{\mathbb{W}}(1), && 0 = \sum_{n=1}^{M} \hat{\mathbb{T}}_n(-1)\check{\mathbb{W}}_n(-1) = \check{\mathbb{W}}(-1),\\
&0 = \sum_{n=1}^{M} \hat{\mathbb{T}}_n(1)\check{\chi}_n(1) = \check{\chi}(1), && 0 = \sum_{n=1}^{M} \hat{\mathbb{T}}_n(-1)\check{\chi}_n(-1) = \check{\chi}(-1),\\
&0 = \sum_{n=1}^{M} \hat{\mathbb{T}}'_n(1)\varpi_n(1) = \check{\mathfrak{D}}\varpi(1), && 0 = \sum_{n=1}^{M} \hat{\mathbb{T}}'_n(-1)\varpi_n(-1) = \check{\mathfrak{D}}\varpi(-1),\\
&0 = \sum_{n=1}^{M} \hat{\mathbb{T}}_n(1)\check{\Theta}_n(1) = \check{\Theta}(1), && 0 = \sum_{n=1}^{M} \hat{\mathbb{T}}_n(-1)\check{\Theta}_n(-1) = \check{\Theta}(-1),\\
&0 = \sum_{n=1}^{M} \hat{\mathbb{T}}_n(1)\check{\Phi}_n(1) = \check{\Phi}(1), && 0 = \sum_{n=1}^{M} \hat{\mathbb{T}}_n(-1)\check{\Phi}_n(-1) = \check{\Phi}(-1).
\end{aligned}
\tag{14}
$$

The generalized eigenvalue system (12) can be solved numerically through the implementation Matlab program employing the QZ algorithm.

5 The Results Discussion

The impacts of the varying gravity, chemical reaction, Brinkman coefficient, the Taylor number, and salt Rayleigh number on the critical Rayleigh number threshold are investigated in this section subject to the fixed border conditions (13). Three various kinds of variable gravity are displayed:

Case A : The linear function, $h_1(z) = -z$.

Case B : The parabolic function, $h_1(z) = -z^2$.

Case C : The exponential function, $h_1(z) = -e^z + 1$.

To verify the precision of the present outcomes, testing calculations are carried out in thermal convection and thermosolutal convection that is saturated in a heated porous medium from below.

For the thermal convection, it can be formally achieved by omitting $(11)_4$ of the system (11) and formally putting $R_s^2 = 0$. The outcomes are compared to those supplied by [15, 7]. In the absence of the Brinkman coefficient effect, $\tilde{\gamma} = 0$ (i.e. Darcy model has been used) depending on free boundary conditions $(14)_{1,4,5}$, where the results in Table 1 recover from those of [15].

Table 1: Contrast of the Ra corresponding critical wave numbers $\check{\mathfrak{a}}_c$ with $R_s^2 = 0$, $h = \eta = 0$, and $\tilde{\gamma} = 0$.

			Current study		[15]	
	α	$\check{T}_a^2$	Ra	$\mathfrak{a}_c$	Ra	$\mathfrak{a}_c$
Case A	0.6	0	56.1434	3.1520	56.1434	3.1517
		100	1710.6869	10.0221	1710.6869	10.0220
		200	3226.3467	11.9113	3226.3467	11.9112
		300	4714.9936	13.1811	4714.9935	13.1812
	0.3	100	1416.2069	9.9703	1416.2069	9.9701
	0.6		1710.6869	10.0221	1710.6869	10.0220
	1.2		2806.7172	10.6032	2806.7173	10.6031
Case B	0.6	0	47.3887	3.1489	47.3887	3.1488
		100	1444.6798	10.0039	1444.6798	10.0037
		200	2724.9140	11.8874	2724.9140	11.8874
		300	3982.3919	13.1540	3982.3919	13.1534
	0.3	100	1315.5033	9.9687	1315.5032	9.9687
	0.6		1444.6798	10.0039	1444.6798	10.0037
	1.2		1774.8683	10.2135	1774.8683	10.2135
Case C	0.6	0	65.2796	3.1795	65.2801	3.1794
		100	1979.7287	10.1846	1979.7424	10.1846
		200	3730.6957	12.1219	3730.7212	12.1219
		300	5449.7517	13.4243	5449.7887	13.4244
	0.3	100	1506.4016	9.9931	1506.4062	9.9930
	0.6		1979.7287	10.1846	1979.7424	10.1846
	1.2		4014.4896	12.5066	4014.5259	12.5067

Table 2: Contrast of the Ra corresponding critical wave numbers $\check{\mathfrak{a}}_c$ with $R_s^2 = 0$, $h = \eta = 0$ and $\alpha = 0$.

	Current study				[7]			
	Ra	$\check{\mathfrak{a}}_c^2$	Ra	$\check{\mathfrak{a}}_c^2$	Ra	$\check{\mathfrak{a}}_c^2$	Ra	$\check{\mathfrak{a}}_c^2$
$\check{T}_a^2$	$\tilde{\gamma} = 0.01$		$\tilde{\gamma} = 0.1$		$\tilde{\gamma} = 0.01$		$\tilde{\gamma} = 0.1$	
0	46.9914	8.5407	108.5734	6.1107	46.991	8.541	108.573	6.111
1	63.3058	11.5517	118.0548	6.7967	63.306	11.552	118.055	6.797
10	27.0450	167.3780	11.0086	182.8851	27.050	167.378	11.009	182.885
10^2	768.9358	94.0092	523.5167	26.8656	768.936	94.011	523.517	26.866
10^3	3790.5113	282.5180	2069.6065	67.2742	3790.511	282.518	2069.606	67.274
	$\tilde{\gamma} = 1$		$\tilde{\gamma} = 10$		$\tilde{\gamma} = 1$		$\tilde{\gamma} = 10$	
0	701.6886	5.094	6619.5020	4.9507	701.689	5.0944	6619.502	4.951
1	703.5013	5.1140	6619.7000	4.9524	703.501	5.114	6619.700	4.952
10	719.5243	5.2834	6621.4815	4.9536	719.524	5.283	6621.481	4.954
10^2	858.8875	6.6888	6639.2574	4.9737	858.887	6.689	6639.257	4.973
10^3	1686.8886	13.3944	6813.2810	5.1672	1686.889	13.394	6813.281	5.167

Furthermore, for the Darcy-Brinkman model based on free boundary conditions (14), the findings in the absence of the variation gravity effect are compared to those provided by [7], and the results in Table 2 match those in [7]. In the rotating thermosolutal convection for the Darcy model where the Brinkman coefficient $\tilde{\gamma}$ is absented (i.e. $\tilde{\gamma} = 0$)with free border conditions (14), the results are recovered from those given by [10].

The calculated results have been achieved for several values of the Brinkman coefficient $\tilde{\gamma}$, the Taylor number $\check{T}_a^2$, the gravity variation coefficient α, the reaction coefficients η, h, and the salt Rayleigh number R_s^2 subject to the fixed border conditions (13). Tables 3−5 and Figures 2−4 show that the Ra grows when $\check{T}_a^2$, α, and $\tilde{\gamma}$ increase. One can note that for $\tilde{\gamma} < 1$ the Ra grows more quickly than for $\tilde{\gamma} \geq 1$ as $\check{T}_a^2$ increases. For example, in Case A at $\alpha = 0.3$, then $Ra = 273.0651$ with $\tilde{\gamma} = 0.1$ and $\check{T}_a^2 = 1$ and $Ra = 1051.3092$ at $\check{T}_a^2 = 100$, as shown in Table 3, while at $\tilde{\gamma} = 10$ and $\check{T}_a^2 = 1$, $Ra = 20227.5958$ and $Ra = 20239.7845$ at $\check{T}_a^2 = 100$. Herein, Cases B and C exhibit similar qualitative behavior in Tables 4 and 5, respectively. It's important to note that for fixed values of α, the outcomes exhibit a qualitative behavior similar to that of [7] in the thermal convection case, as seen in Table 2.

Table 3: Contrast of the Ra corresponding critical wave numbers $\check{\mathfrak{a}}_c$ with $R_s^2 = 9$, $h = 9$ and $\eta = 6$ for Case A.

		Ra	$\check{\mathfrak{a}}_c$	Ra	$\check{\mathfrak{a}}_c$	Ra	$\check{\mathfrak{a}}_c$	Ra	$\check{\mathfrak{a}}_c$
α	$\check{T}_a^2$	$\tilde{\gamma} = 0.01$		$\tilde{\gamma} = 0.1$		$\tilde{\gamma} = 1$		$\tilde{\gamma} = 10$	
0.3	0	78.5963	3.2200	265.01955	3.1820	2090.9327	3.1320	20227.4726	3.1210
	1	99.2973	3.2200	273.0651	3.2200	2092.1088	3.1330	20227.5958	3.1210
	10	279.07867	3.2200	344.8328	3.2200	2102.6555	3.1430	20228.7040	3.1210
	10^2	2008.0353	3.2200	1051.3092	3.2200	2204.7034	3.2200	20239.7845	3.1220
	10^3	19049.5831	3.2200	7911.14268	3.2200	3205.6589	3.2200	20350.1388	3.1340
0.6	0	94.1109	3.2200	319.7595	3.1810	2532.3698	3.1320	24523.2349	3.1220
	1	119.1098	3.2200	329.4924	3.2200	2533.7936	3.1330	24523.3840	3.1220
	10	336.3776	3.2200	416.2816	3.2200	2546.5601	3.1440	24524.7259	3.1220
	10^2	2428.0579	3.2200	1270.2460	3.2200	2670.0900	3.2200	24538.1397	3.1230
	10^3	23056.3969	3.2200	9558.2621	3.2200	3881.7734	3.2200	24671.7263	3.1350
0.9	0	117.4587	3.2200	403.0245	3.1840	3205.9468	3.1360	31082.6072	3.1260
	1	148.9116	3.2200	415.2842	3.2200	3207.7412	3.1370	31082.7952	3.1270
	10	422.4594	3.2200	524.6713	3.2200	3223.8291	3.1480	31084.4861	3.1270
	10^2	3058.6526	3.2200	1598.5123	3.2200	3379.5691	3.2200	31101.3918	3.1280
	10^3	29071.8542	3.2200	11993.5698	3.2200	4908.4020	3.2200	31269.7561	3.1400
1.2	0	155.8873	3.2200	543.3601	3.2010	4348.2087	3.1510	42218.4845	3.1420
	1	197.8869	3.2200	559.7299	3.2200	4350.6002	3.1520	42218.7351	3.1420
	10	563.2998	3.2200	706.1341	3.2200	4372.0397	3.1630	42220.9899	3.1420
	10^2	4087.3126	3.2200	2132.5813	3.2200	4580.1640	3.2200	42243.5295	3.1430
	10^3	38878.4443	3.2200	15829.1232	3.2200	6628.5768	3.2200	42467.9711	3.1550

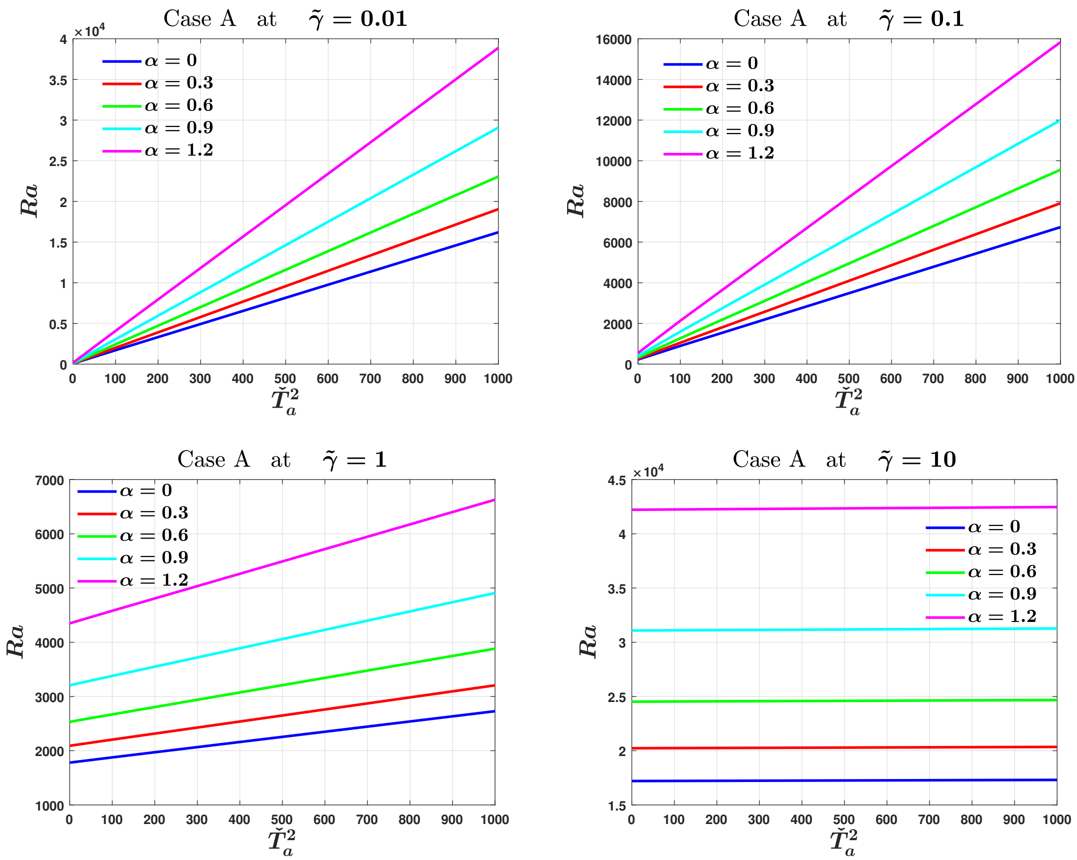

Figure 2: The threshold of linear instability's critical Rayleigh number for various values of α, $\tilde{\gamma}$ and $\check{T}_a^2$ at $R_s^2 = 9$, $h = 9$ and $\eta = 6$ for Case A.

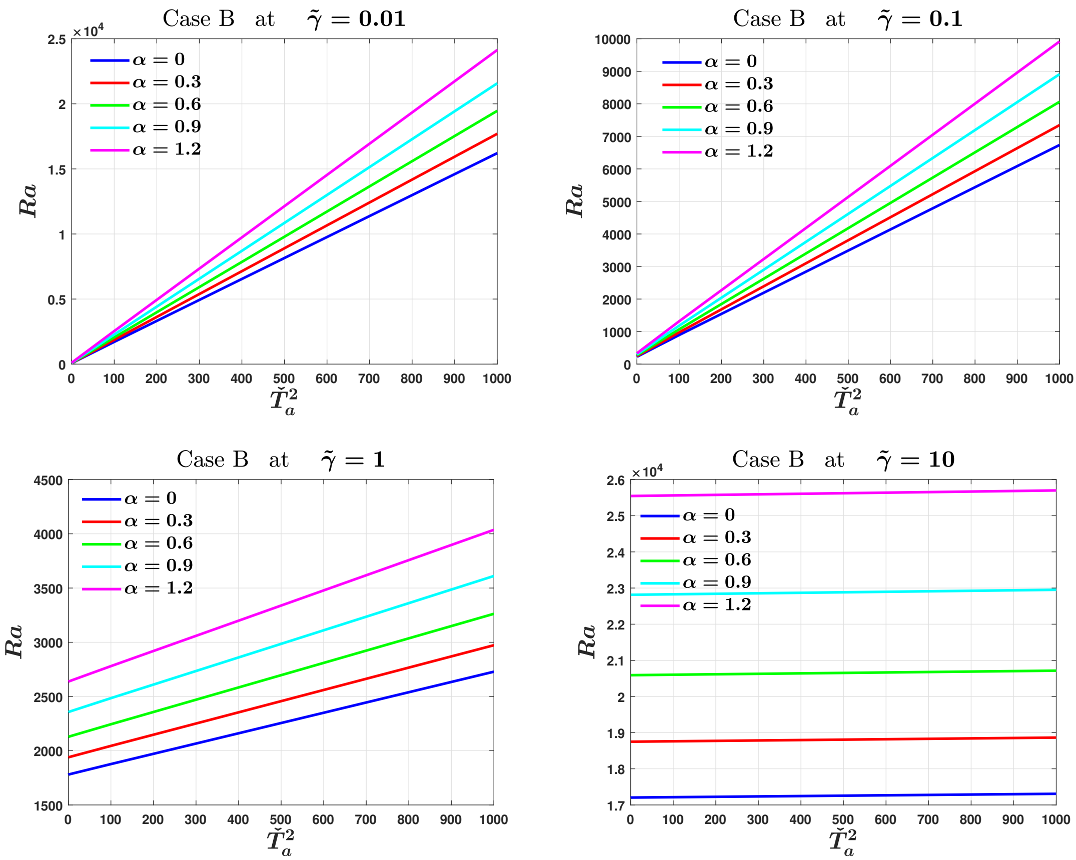

Figure 3: The threshold of linear instability's critical Rayleigh number for various values of α, $\tilde{\gamma}$ and $\check{T}_a^2$ at $R_s^2 = 9$, $h = 9$ and $\eta = 6$ for Case B.

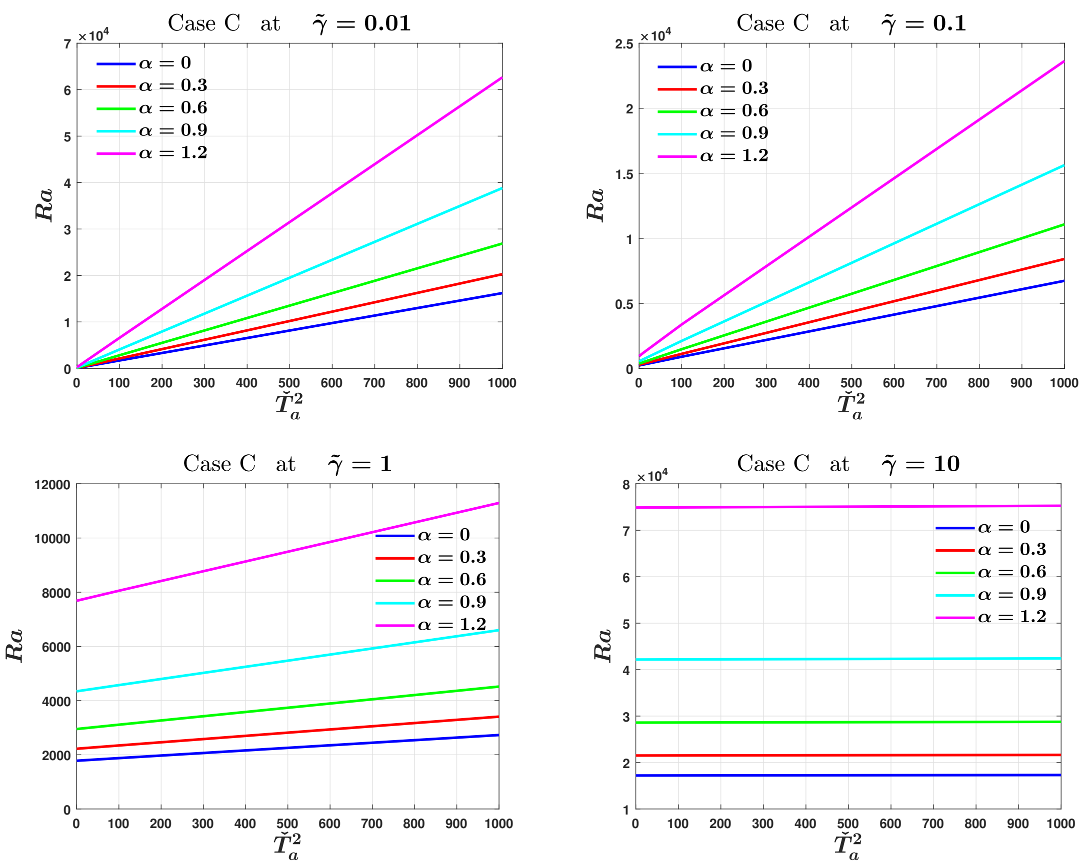

Figure 4: The threshold of linear instability's critical Rayleigh number for various values of α, $\tilde{\gamma}$ and $\check{T}_a^2$ at $R_s^2 = 9$, $h = 9$ and $\eta = 6$ for Case C.

When α increases , the Rayleigh number grows faster for $\tilde{\gamma} \geq 1$ than for $\tilde{\gamma} < 1$. As an illustration, in Case A at $\check{T}_a^2 = 10$, then $Ra = 259.5350$ as $\tilde{\gamma} = 0.01$ and $\alpha = 0.3$ and $Ra = 350.6596$ with $\alpha = 1.2$, as seen in Table 3, whereas at $\tilde{\gamma} = 1$ and $\alpha = 0.3$, $Ra = 1949.8670$ and at $\alpha = 1.2$ then $Ra = 2651.9461$. Also, in Tables 4 and 5, similar behavior are manifested in Cases B and C, respectively.

Table 4: Contrast of the Ra corresponding critical wave numbers $\breve{\mathfrak{a}}_c$ with $R_s^2 = 9$, $h = 9$ and $\eta = 6$ for Case B.

α	$\breve{T}_a^2$	Ra	$\breve{\mathfrak{a}}_c$	Ra	$\breve{\mathfrak{a}}_c$	Ra	$\breve{\mathfrak{a}}_c$	Ra	$\breve{\mathfrak{a}}_c$
		$\tilde{\gamma} = 0.01$		$\tilde{\gamma} = 0.1$		$\tilde{\gamma} = 1$		$\tilde{\gamma} = 10$	
0.3	0	73.2525	3.2200	246.1614	3.1830	1938.9994	3.1320	18749.5053	3.1210
	1	92.4869	3.2200	253.6231	3.2200	1940.0898	3.1330	18749.6195	3.1210
	10	259.5350	3.2200	320.2064	3.2200	1949.8670	3.1440	18750.6468	3.1210
	10^2	1865.8294	3.2200	975.8093	3.2200	2044.4745	3.2200	18760.9187	3.1220
	10^3	17696.1180	3.2200	7345.9584	3.2200	2972.6019	3.2200	18863.2202	3.1340
0.6	0	79.9505	3.2200	269.6504	3.1830	2128.1578	3.1320	20589.6755	3.1210
	1	101.0586	3.2200	277.8363	3.2200	2129.3543	3.1330	20589.8008	3.1210
	10	284.5247	3.2200	350.8758	3.2200	2140.0821	3.1440	20590.9286	3.1210
	10^2	2050.3589	3.2200	1070.1375	3.2200	2243.8916	3.2200	20602.1998	3.1230
	10^3	19460.1055	3.2200	8063.3946	3.2200	3262.3826	3.2200	20714.4487	3.1340
0.9	0	87.9663	3.2200	297.9634	3.1840	2356.6315	3.1340	22813.2593	3.1230
	1	111.3162	3.2200	307.0112	3.2200	2357.9540	3.1350	22813.3978	3.1230
	10	314.4388	3.2200	387.7657	3.2200	2369.8121	3.1460	22814.6445	3.1230
	10^2	2271.4045	3.2200	1182.6065	3.2200	2484.5799	3.2200	22827.1038	3.1250
	10^3	21573.8451	3.2200	8910.9439	3.2200	3611.0362	3.2200	22951.1845	3.1360
1.2	0	97.6782	3.2200	332.6396	3.1880	2637.2601	3.1380	25545.9076	3.1270
	1	123.7408	3.2200	342.7233	3.2200	2638.7337	3.1390	25546.0619	3.1270
	10	350.6596	3.2200	432.7989	3.2200	2651.9461	3.1500	25547.4510	3.1280
	10^2	2539.1254	3.2200	1318.0491	3.2200	2779.8870	3.2200	25561.3343	3.1290
	10^3	24134.4835	3.2200	9917.0321	3.2200	4036.7450	3.2200	25699.5993	3.1400

Table 5: Contrast of the Ra corresponding critical wave numbers $\breve{\mathfrak{a}}_c$ with $R_s^2 = 9$, $h = 9$ and $\eta = 6$ for Case C.

α	$\breve{T}_a^2$	Ra	$\breve{\mathfrak{a}}_c$	Ra	$\breve{\mathfrak{a}}_c$	Ra	$\breve{\mathfrak{a}}_c$	Ra	$\breve{\mathfrak{a}}_c$
		$\tilde{\gamma} = 0.01$		$\tilde{\gamma} = 0.1$		$\tilde{\gamma} = 1$		$\tilde{\gamma} = 10$	
0.3	0	83.2546	3.2200	281.3470	3.1820	2222.4437	3.1320	21506.9880	3.1210
	1	105.2611	3.2200	289.8964	3.2200	2223.6937	3.1330	21507.1189	3.1210
	10	296.4897	3.2200	366.1563	3.2200	2234.9018	3.1440	21508.2971	3.1210
	10^2	2136.7627	3.2200	1116.9662	3.2200	2343.3526	3.2200	21520.0732	3.1220
	10^3	20280.6228	3.2200	8411.5049	3.2200	3407.1779	3.2200	21637.3490	3.1340
0.6	0	108.6133	3.2200	371.4248	3.1850	2950.3911	3.1370	28594.0765	3.1270
	1	137.6644	3.2200	382.7111	3.2200	2952.0419	3.1380	28594.2493	3.1270
	10	390.4647	3.2200	483.4559	3.2200	2966.8435	3.1490	28595.8050	3.1270
	10^2	2827.7082	3.2200	1473.1803	3.2200	3110.1412	3.2200	28611.3585	3.1280
	10^3	26878.5341	3.2200	11071.5710	3.2200	4517.1780	3.2200	28766.2556	3.1400
0.9	0	154.9788	3.2200	542.0524	3.2150	4342.1785	3.1630	42166.1892	3.1530
	1	196.7974	3.2200	558.2640	3.2200	4344.5344	3.1640	42166.4361	3.1530
	10	561.1232	3.2200	703.3473	3.2200	4365.6541	3.1750	42168.6580	3.1540
	10^2	4078.9244	3.2200	2112.3393	3.2200	4571.3697	3.2200	42190.8652	3.1550
	10^3	38820.8696	3.2200	15627.5637	3.2200	6599.4968	3.2200	42411.9966	3.1670
1.2	0	252.0023	3.2200	940.8794	3.2200	7683.8417	3.2200	74882.3660	3.2200
	1	319.5864	3.2200	967.0787	3.2200	7687.5557	3.2200	74882.7531	3.2200
	10	907.9543	3.2200	1199.3989	3.2200	7720.9700	3.2200	74886.2371	3.2200
	10^2	6584.8650	3.2200	3374.1028	3.2200	8054.0059	3.2200	74921.0761	3.2200
	10^3	62653.5296	3.2200	23631.3078	3.2200	11293.2832	3.2200	75269.3392	3.2200

In Figure 5, for different values of h, η, and R_s^2, anybody can note that when $h \leq \eta$ and R_s^2 increases, the critical Rayleigh number slowly grows, while when $h > \eta$, the critical Rayleigh number grows more quickly than when $h \leq \eta$. It's important to note that in all the calculations performed, it has been found that in Case C, Ra grows faster than in Cases A and B.

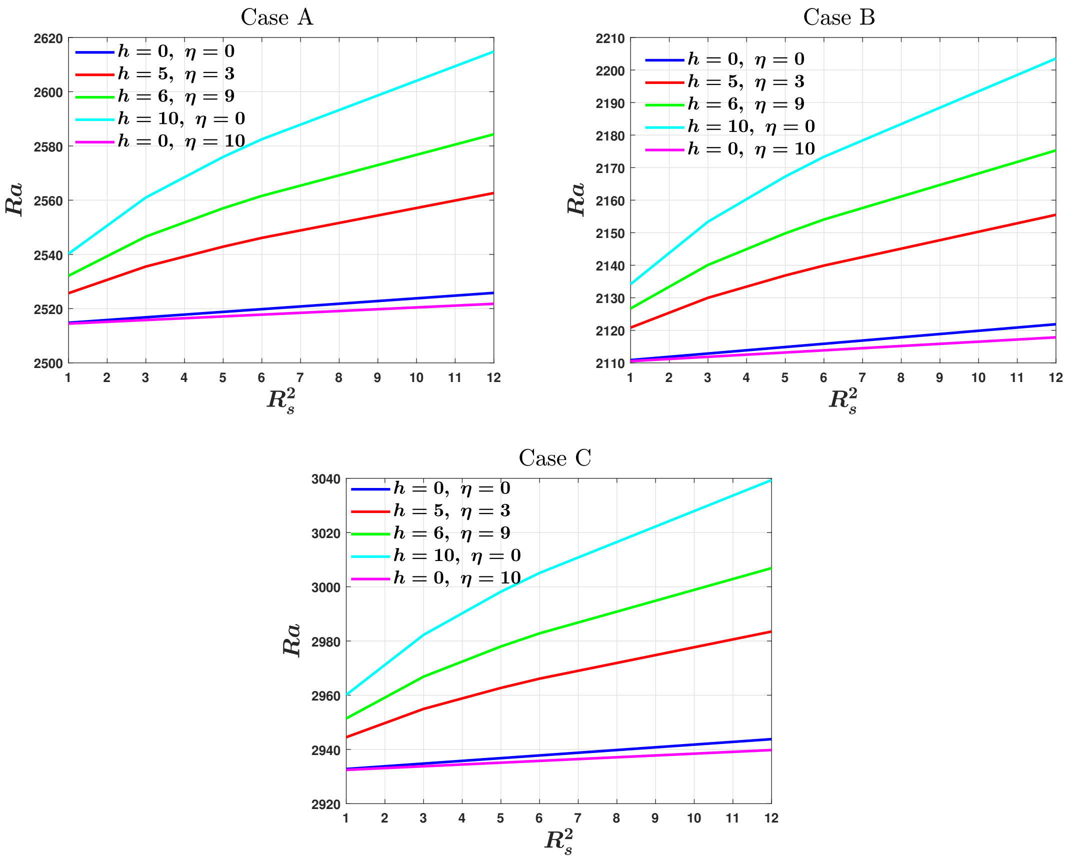

Figure 5: The threshold of linear instability's critical Rayleigh number for $h = \eta$, $h > \eta$, $h < \eta$ and various values of R_s^2 at $\alpha = 0.6$, $\tilde{\gamma} = 1$ and $\check{T}_a^2 = 10$.

Despite the linear critical Rayleigh numbers increasing fast when the Brinkman coefficient value is large, the results of the effects of the chemical reaction, varying gravity, Taylor number, and salt Rayleigh number with fixed border conditions could be concluded to have qualitative behavior similar to work given by [10] under free border conditions (14) and in the absence of the Brinkman coefficient effect.

6 Conclusions

The influences of varying gravity, rotation, Brinkman, and chemical reaction coefficients have been explored in detail on the system's instability in this study. Thermosolutal-convection in a porous substance for the Darcy-Brinkman problem is studied when the bottom layer has been heated and salted. The linear instability theory has been analyzed to determine the influence of several factors on the system's instability. To obtain computational outcomes, the D^2 Chebyshev Tau technique has been applied. Three different functions of varying gravity have been discussed: the linear function, the parabolic function, and the exponential function. Hence, one can conclude the following:

1. It has been found that the downward gravitational and rotational effects improved the arrangement's stability. The scope of the convective cells decreased as the gravity variation and rotation parameters increased. It has also been discovered that the system is more disturbed when the variable gravity field is in the second case, whereas it is more stable in the third case.

2. For a certain Brinkman coefficient $\tilde{\gamma}$, the critical Rayleigh number grows as $\check{T}_a^2$ increases, whereas for large $\check{T}_a^2$, the critical Rayleigh number decreases with the parameter $\tilde{\gamma}$ and then increases for large $\tilde{\gamma}$. The critical Rayleigh number increases faster for small $\tilde{\gamma}$ than for large $\tilde{\gamma}$ coefficients, as shown in the homogeneous fluid case in reference [7].

3. For the effects of chemical reaction and salt Rayleigh number on the stability of the arrangement, one may argue from the results is to grow the critical Rayleigh number with the increasing of chemical reaction parameters and salt Rayleigh number especially when h is greater than η.

4. Comparing the current study with the previous study [10], in the current work, the linear critical Rayleigh numbers are growing rapidly when the value of the Brinkman coefficient is higher.

Acknowledgement The author sincerely acknowledges the support and contributions of all individuals and institutions involved in this work.

Conflicts of Interest The author declare no conflict of interest.

References

[1] D. Bains, P. L. Sharma & G. C. Rana (2024). Effect of variable gravity on thermal convection in rotating Jeffrey nanofluid: Darcy-Brinkman model. *Special Topics & Reviews in Porous Media: An International Journal*, *15*(5), 25–40. https://doi.org/10.1615/SpecialTopicsRevPorousMedia.2023049875.

[2] S. Chandrasekhar (1981). *Hydrodynamic and Hydromagnetic Stability*. Dover Books on Physics Series. Dover Publications, New York.

[3] J. J. Dongarra, B. Straughan & D. W. Walker (1996). Chebyshev tau-QZ algorithm methods for calculating spectra of hydrodynamic stability problems. *Applied Numerical Mathematics*, *22*(4), 399–434. https://doi.org/10.1016/S0168-9274(96)00049-9.

[4] F. Franchi & B. Straughan (2001). A comparison of the Graffi and Kazhikhov–Smagulov models for top heavy pollution instability. *Advances in Water Resources*, *24*(6), 585–594. https://doi.org/10.1016/S0309-1708(00)00073-7.

[5] R. Idris, A. Alias & A. Miqdady (2023). Behaviour of the onset of Rayleigh-Bénard convection in double-diffusive micropolar fluids under the influence of cubic temperature and

concentration gradient. *Malaysian Journal of Mathematical Sciences*, *17*(3), 441–458. https://doi.org/10.47836/mjms.17.3.12.

[6] I. K. Khalid, N. F. M. Mokhtar, Z. Siri, Z. B. Ibrahim & S. S. Abd Gani (2019). Magneto-convection on the double-diffusive nanofluids layer subjected to internal heat generation in the presence of Soret and Dufour effects. *Malaysian Journal of Mathematical Sciences*, *13*(3), 397–418.

[7] S. Lombardo & G. Mulone (2002). Necessary and sufficient conditions of global nonlinear stability for rotating double-diffusive convection in a porous medium. *Continuum Mechanics and Thermodynamics*, *14*, 527–540. https://doi.org/10.1007/s001610200091.

[8] S. Lombardo, G. Mulone & B. Straughan (2001). Non-linear stability in the Bénard problem for a double-diffusive mixture in a porous medium. *Mathematical Methods in the Applied Sciences*, *24*(16), 1229–1246. https://doi.org/10.1002/mma.263.

[9] N. J. Noon & S. A. Haddad (2023). The combined effect of variable gravity and internal heat source on the double diffusive convection with the effect of reaction and slip boundary. In *AIP Conference Proceedings*, volume 2834 of *2nd International Conference of Mathematics, Applied Sciences, Information and Communication Technology* pp. Article ID: 080108. Baghdad, Iraq. AIP Publishing. https://doi.org/10.1063/5.0161503.

[10] N. J. Noon & S. A. Haddad (2022). Stability analysis for rotating double-diffusive convection in the presence of variable gravity and reaction effects: Darcy model. *Special Topics & Reviews in Porous Media: An International Journal*, *13*(4), 1–22. https://doi.org/10.1615/SpecialTopicsRevPorousMedia.2022042776.

[11] N. J. Noon & S. A. Haddad (2023). Magnetic and chemical reaction effects on double-diffusive convection with the effect of heat and salt flux boundary conditions. *Heat Transfer*, *52*(7), 4895–4913. https://doi.org/10.1002/htj.22910.

[12] D. Pritchard & C. N. Richardson (2007). The effect of temperature-dependent solubility on the onset of thermosolutal convection in a horizontal porous layer. *Journal of Fluid Mechanics*, *571*, 59–95. https://doi.org/10.1017/S0022112006003211.

[13] P. L. Sharma, D. Bains & G. C. Rana (2024). Effect of variable gravity on thermal convection in Jeffrey nanofluid: Darcy-Brinkman model. *Numerical Heat Transfer, Part B: Fundamentals*, *85*(6), 776–790. https://doi.org/10.1080/10407790.2023.2256970.

[14] B. Straughan (2001). A sharp nonlinear stability threshold in rotating porous convection. *Proceedings of the Royal Society of London. Series A: Mathematical, Physical and Engineering Sciences*, *457*(2005), 87–93. https://doi.org/10.1098/rspa.2000.0657.

[15] D. Yadav (2020). Effects of rotation and varying gravity on the onset of convection in a porous medium layer: A numerical study. *World Journal of Engineering*, *17*(6), 785–793. https://doi.org/10.1108/WJE-03-2020-0086.